Dynamical origin for the occurrence of asynchronous hyperchaos and chaos via blowout bifurcations

Sang-Yoon Kim,[1,2,*] Woochang Lim,[2] Edward Ott,[1,3] and Brian Hunt[4]
[1]*Institute for Research in Electronics and Applied Physics, University of Maryland, College Park, Maryland 20742, USA*
[2]*Department of Physics, Kangwon National University, Chunchon, Kangwon-Do 200-701, Korea*
[3]*Department of Physics and Department of Electrical and Computing Engineering, University of Maryland, College Park, Maryland 20742, USA*
[4]*Institute for Physical Science and Technology and Department of Mathematics, University of Maryland, College Park, Maryland 20742, USA*

(Received 17 January 2003; revised manuscript received 29 July 2003; published 17 December 2003)

We investigate the dynamical origin for the occurrence of asynchronous hyperchaos and chaos via blowout bifurcations in coupled chaotic systems. An asynchronous hyperchaotic or chaotic attractor with a positive or negative second Lyapunov exponent appears through a blowout bifurcation. It is found that the sign of the second Lyapunov exponent of the newly born asynchronous attractor, exhibiting on-off intermittency, is determined through competition between its laminar and bursting components. When the ''strength'' (i.e., a weighted second Lyapunov exponent) of the bursting component is larger (smaller) than that of the laminar component, an asynchronous hyperchaotic (chaotic) attractor appears.

DOI: 10.1103/PhysRevE.68.066203 PACS number(s): 05.45.Xt

I. INTRODUCTION

Recently, because of its potential practical applications (e.g., see Ref. [1]), the phenomenon of synchronization in coupled chaotic systems has become a field of intensive study. When identical chaotic systems synchronize, chaotic motion may occur on an invariant subspace of the whole phase space [2–5]. An important problem concerns the stability of chaos synchronization [6,7]. When the Lyapunov exponents corresponding to perturbations transverse to the invariant synchronization subspace are all negative, the synchronous chaotic state is stable, and is an attractor in the whole phase space. However, as a coupling parameter passes a threshold value, the synchronized chaotic attractor (SCA) can become transversely unstable (i.e., its largest transverse Lyapunov exponent becomes positive), and desynchronization occurs via a blowout bifurcation [8–11]. Depending on the global dynamics, two kinds of blowout bifurcations may occur. For the case of a supercritical (nonhysteretic) blowout bifurcation, an asynchronous attractor is born, and exhibits intermittent bursting, called on-off intermittency [12–20]; long periods of nearly synchronous motion (off state) are occasionally interrupted by short-term asynchronous burstings (on state). On the other hand, for the case of a subcritical (hysteretic) blowout bifurcation, an abrupt disappearance of the synchronized state occurs, and typical trajectories starting near the invariant subspace are attracted to another distant asynchronous attractor (or infinity).

Here, we are interested in the type of asynchronous intermittent attractors born via supercritical blowout bifurcations. In particular, we are interested in whether the intermittent bursting attractor born at the blowout bifurcation is hyperchaotic (i.e., has more than one positive Lyapunov exponent) or not. Examples of both hyperchaotic attractors [9,21,22] and chaotic attractors (i.e., an attractor with only one positive Lyapunov exponent) [9,23] were given in previous works. However, the dynamical origin for the appearance of such asynchronous hyperchaotic and chaotic bursting attractors remains unclear.

In this paper, we investigate the dynamical origin for the occurrence of asynchronous hyperchaos and chaos via blowout bifurcations in coupled chaotic systems. As a representative model, we consider a system of two coupled one-dimensional (1D) maps with a parameter α tuning the degree of asymmetry of coupling [23]. This model system can be used to represent the two-cluster dynamics in globally coupled 1D maps [24], in which each element is coupled to all others with equal strength, and the asymmetry parameter α is related to a parameter describing the distribution of elements between the two clusters. We also note that for many-coupled case, this kind of asymmetrically coupled maps are usually used to model the open flow systems with a preferred direction of propagation [25]. Depending on the value of α, an asynchronous hyperchaotic or chaotic attractor appears through a blowout bifurcation. This transition to asynchronous hyperchaos or chaos via a blowout bifurcation corresponds to a transition from a fully synchronized state to a hyperchaotic or chaotic two-cluster state in globally coupled 1D maps. In Sec. II, we study the type of asynchronous intermittent attractors born via blowout bifurcations in two coupled 1D maps by varying the asymmetry parameter α. Experimental examples of asymmetric and symmetric couplings are provided by Refs. [26,27] that investigate two chaotic electronic circuits with unidirectional and symmetric couplings, respectively. A typical trajectory on the newly born asynchronous attractor, exhibiting on-off intermittency, may be decomposed into laminar (i.e., nearly synchronous) and bursting components. It is found that the type of the asynchronous intermittent attractor (corresponding to an in-

*Electronic address: sykim@kangwon.ac.kr

 ©2003 The American Physical Society

termittent two-cluster state for the case of global coupling) may be determined through competition between its laminar and bursting components. When the ''strength'' (i.e., its weighted second Lyapunov exponent) of the bursting component is larger (smaller) than that of the laminar component, an asynchronous hyperchaotic (chaotic) attractor [corresponding to a hyperchaotic (chaotic) two-cluster state for the globally coupled case] appears. These results are of wider significance because the (uncoupled) 1D map is a paradigm model for period-doubling dynamics in a large class of systems. As examples, we consider coupled Hénon maps [17] and coupled parametrically forced pendula [28], which are high-dimensional invertible period-doubling systems, and obtain similar results. Finally, a summary is given in Sec. III.

II. TYPE OF ASYNCHRONOUS INTERMITTENT ATTRACTORS BORN VIA BLOWOUT BIFURCATIONS

A. Consequence of blowout bifurcations in two coupled 1D maps

In this section we investigate the dynamical origin for the appearance of asynchronous hyperchaotic and chaotic attractors via blowout bifurcations in a representative model system of two coupled 1D maps with a parameter α tuning the asymmetry of coupling. The asymmetric coupling naturally appears in the dynamics of two clusters for the case of global coupling [24], in which each element is coupled to all the other elements with equal strength. Examples of globally coupled systems are laser arrays [29], Josephson junction arrays [30], cardiac pacemaker cells [31], flashing fireflies [32], and chirping crickets [33]. As a basic model, we consider N globally coupled 1D maps [34],

$$x_i(t+1)=f(x_i(t))+\frac{\varepsilon}{N}\sum_{j=1}^{N}[f(x_j(t))-f(x_i(t))], \quad (1)$$

where $x_i(t)$ is a state variable of the ith element at a discrete time t, the uncoupled dynamics ($\varepsilon=0$) is governed by the 1D map $f(x)=1-ax^2$ with a control parameter a, and ε is a coupling parameter. For certain values of ε, full synchronization in which all elements exhibit the same temporal behaviors [i.e., $x_1(t)=\cdots=x_N(t)$] occurs. For other values of ε, the population of elements splits into groups with different dynamics. For example, in the case of two clusters, we have

$$x_{i_1}(t)=x_{i_2}(t)=\cdots=x_{i_{N_1}}(t)\equiv x_t,$$

$$x_{i_{N_1+1}}(t)=x_{i_{N_1+2}}(t)=\cdots=x_{i_N}(t)\equiv y_t, \quad (2)$$

where N_1 and N_2 ($=N-N_1$) represent the number of elements in the first and second clusters, exhibiting the x and y dynamics, respectively. This two-cluster state is a usual clustering to occur when the full synchronization breaks down. Under condition (2), the system of globally coupled 1D maps is reduced to a system of two coupled 1D maps with a parameter p describing the distribution of elements between the two clusters [24],

$$x_{t+1}=f(x_t)+p\varepsilon[f(y_t)-f(x_t)],$$

$$y_{t+1}=f(y_t)+(1-p)\varepsilon[f(x_t)-f(y_t)], \quad (3)$$

where $p=N_2/N$ ($0\leqslant p\leqslant 1$) denotes the fraction of the total population of elements in the second cluster. Note that an uneven distribution of elements between the two clusters causes an asymmetry in the coupling. Since the two coupled maps (3) are invariant under the interchange of x and y ($x\leftrightarrow y$) and a change of p ($p\rightarrow 1-p$), it is sufficient to consider only the case of $0\leqslant p\leqslant 1/2$. Furthermore, through a transformation of parameters

$$p\rightarrow\frac{1-\alpha}{2-\alpha} \quad \text{and} \quad \varepsilon\rightarrow(2-\alpha)c, \quad (4)$$

we obtain two coupled 1D maps T, which were used in our previous work [23],

$$T:\begin{cases} x_{t+1}=f(x_t)+(1-\alpha)c[f(y_t)-f(x_t)] \\ y_{t+1}=f(y_t)+c[f(x_t)-f(y_t)]. \end{cases} \quad (5)$$

Here, c is a coupling parameter and α ($0\leqslant\alpha\leqslant 1$) is a parameter tuning the degree of asymmetry of coupling from symmetric coupling ($\alpha=0$) to unidirectional coupling ($\alpha=1$). Consequently, Eq. (5) may be used as a model map for studying a transition from full synchronization to two-cluster dynamics in globally coupled systems.

The coupled map T has an invariant synchronization line $x=y$. If an orbit lies on this invariant diagonal, then it is called a synchronous orbit because the state variables x_t and y_t become the same for all t; otherwise it is called an asynchronous orbit. For the accuracy of numerical calculations [35], we introduce new coordinates, u and v,

$$u=\frac{x+y}{2}, \quad v=\frac{x-y}{2}. \quad (6)$$

Under the coordinate change, the invariant diagonal $x=y$ is transformed into a new invariant line $v=0$. In these new coordinates, the coupled map T of Eq. (5) becomes

$$T:\begin{cases} u_{t+1}=1-a(u_t^2+v_t^2)-2a\alpha c u_t v_t \\ v_{t+1}=-2a[1-(2-\alpha)c]u_t v_t. \end{cases} \quad (7)$$

From now on, we investigate the dynamical origin for the occurrence of asynchronous hyperchaos and chaos via blowout bifurcations in the new map T by varying the asymmetry parameter α.

We also note that the coupled map T is noninvertible, because its Jacobian determinant $\det(DT)$ (DT is the Jacobian matrix of T) becomes zero along the critical curves, $C_0=\{(u,v)\in R^2: u=v \text{ or } u=-v\}$. Critical curves of rank k, C_k ($k=1,2,\ldots$), are then given by the images of C_0 [i.e., $C_k=T^k(C_0)$]. Segments of these critical curves can be used to bound a compact region of the phase space that acts as a trapping bounded vessel, called an absorbing area $\mathcal{A}$, inside which trajectories bursting away from the invariant line $v=0$ are confined [36,37]. Furthermore, boundaries of such an

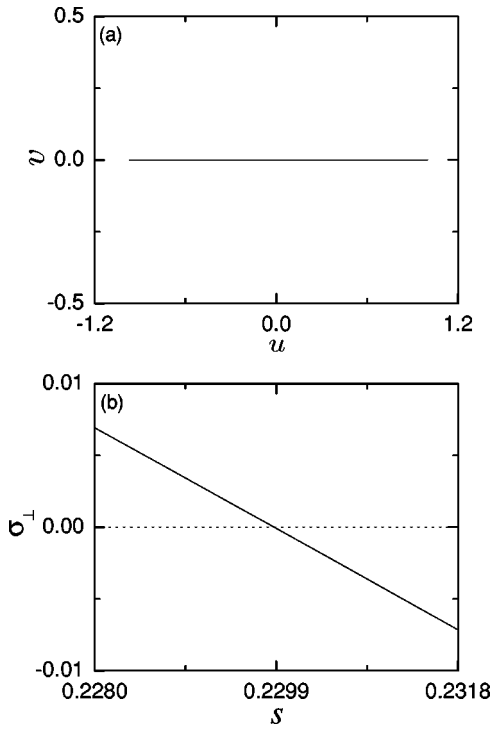

FIG. 1. (a) One-band SCA on the invariant line $v=0$ for $a=1.97$ and $s[\equiv(1-\alpha/2)c]=0.23$. (b) Plot of the transverse Lyapunov exponent $\sigma_\perp$ of the SCA vs the scaled coupling parameter s. As s decreases through a threshold value s^* ($\simeq 0.2299$), $\sigma_\perp$ becomes positive.

absorbing area can also be obtained by the union of segments of critical curves and portions of unstable manifolds of unstable periodic orbits. For this case, $\mathcal{A}$ is called a mixed absorbing area. We note that the consequence of the blowout bifurcation of the SCA depends on the existence of an absorbing area, controlling the global dynamics. In the presence of an absorbing area, an asynchronous attractor within this absorbing area is born through a supercritical blowout bifurcation. However, in the absence of an absorbing area, an abrupt change from the synchronized state occurs via a subcritical blowout bifurcation, because almost all points near the invariant line $v=0$ eventually move away and never return.

With increase of the control parameter a, the coupled map T exhibits an infinite sequence of period-doubling bifurcations of synchronous attractors with period 2^n ($n=0,1,2,\ldots$), ending at the accumulation point a_∞ ($=1.401\,155\ldots$), in some region of c. This period-doubling cascade leads to creation of the SCA on the invariant line $v=0$. With further increase of a past a_∞, a sequence of band-merging bifurcations of the SCA takes place. Hereafter, we fix the value of a as $a=1.97$, where a single-band SCA exists on the invariant $v=0$ line, as shown in Fig. 1(a). The longitudinal stability of trajectories on the SCA against perturbation along the $v=0$ line is determined by its longitudinal Lyapunov exponent

$$\sigma_{||}=\lim_{N\to\infty}\frac{1}{N}\sum_{t=1}^{N}\ln|2au_t|, \tag{8}$$

which is just the Lyapunov exponent in the uncoupled 1D map. For $a=1.97$, we have $\sigma_{||}=0.6157$. On the other hand, the transverse stability of the SCA against perturbation across the $v=0$ line is determined by its transverse Lyapunov exponent, which for the map T is given by

$$\sigma_\perp=\sigma_{||}+\ln|1-2s|, \tag{9}$$

where s $[\equiv(1-\alpha/2)c]$ is a scaled coupling parameter. A plot of $\sigma_\perp$ versus s is shown in Fig. 1(b). If s is relatively large such that $\sigma_{||}<-\ln(1-2s)$, then the SCA becomes transversely stable (i.e., its transverse Lyapunov exponent $\sigma_\perp$ is negative). Intuitively, this result seems to make sense since strongly coupled systems tend to synchronize. However, as s is decreased and passes a threshold value s^*,

$$s^*=\tfrac{1}{2}(1-e^{-\sigma_{||}}), \tag{10}$$

the transverse Lyapunov exponent $\sigma_\perp$ of the SCA becomes positive. For $a=1.97$, we have $s^*\simeq 0.2299$. Consequently, when passing s^*, the SCA becomes transversely unstable, and then an asynchronous attractor, filling an absorbing area, is born through a supercritical blowout bifurcation.

To determine the type of a newly born asynchronous attractor, its Lyapunov exponents are numerically calculated as follows. We choose a random initial orbit point with uniform probability in the range of $u\in(1-a,1)$ on a line $v=\varepsilon$ ($\varepsilon=10^{-6}$) near the invariant line $v=0$ and follow the trajectory until its length L becomes 10^8 [38]. Then we obtain the Lyapunov exponents through the Gram-Schmidt reorthonormalization (GSR) procedure [39]. For a trajectory segment, we consider the evolution of a set of two orthonormal tangent vectors $\{\mathbf{z}_t^{(1)},\mathbf{z}_t^{(2)}\}$ along the trajectory $\{\mathbf{w}_t[\equiv(u_t,v_t)]\}$ ($t=0,1,2,\ldots$). By an application of the linearized map $DT(\mathbf{w}_t)$ (i.e., Jacobian matrix of T at the orbit point $\mathbf{w}_t$) on $\{\mathbf{z}_t^{(1)},\mathbf{z}_t^{(2)}\}$, we obtain a set of two evolved tangent vectors, $\{DT(\mathbf{w}_t)\mathbf{z}_t^{(1)},DT(\mathbf{w}_t)\mathbf{z}_t^{(2)}\}$. At each time step, we replace the evolved tangent vectors with a new set of reorthonormalized tangent vectors $\{\mathbf{z}_{t+1}^{(1)},\mathbf{z}_{t+1}^{(2)}\}$ using the GSR method:

$$\mathbf{z}_{t+1}^{(1)}=\frac{DT(\mathbf{w}_t)\mathbf{z}_t^{(1)}}{d_{t+1}^{(1)}},\quad \mathbf{z}_{t+1}^{(2)}=\frac{\mathbf{q}_{t+1}^{(2)}}{d_{t+1}^{(2)}}, \tag{11a}$$

$$d_{t+1}^{(1)}=||DT(\mathbf{w}_t)\mathbf{z}_t^{(1)}||=\sqrt{\langle DT(\mathbf{w}_t)\mathbf{z}_t^{(1)},DT(\mathbf{w}_t)\mathbf{z}_t^{(1)}\rangle}, \tag{11b}$$

$$d_{t+1}^{(2)}=||\mathbf{q}_{t+1}^{(2)}||=\sqrt{\langle\mathbf{q}_{t+1}^{(2)},\mathbf{q}_{t+1}^{(2)}\rangle}, \tag{11c}$$

$$\mathbf{q}_{t+1}^{(2)}=DT(\mathbf{w}_t)\mathbf{z}_t^{(2)}-\langle DT(\mathbf{w}_t)\mathbf{z}_t^{(2)},\mathbf{z}_{t+1}^{(1)}\rangle\mathbf{z}_{t+1}^{(1)}, \tag{11d}$$

where $\langle,\rangle$ denotes the inner product of two vectors and $d_{t+1}^{(1)}$ ($d_{t+1}^{(2)}$) represents the length of the evolved first vector (the component of the evolved second vector orthogonal to the evolved first vector, i.e., $\mathbf{q}_{t+1}^{(2)}$). Note that the GSR never affects the direction of the first vector $\mathbf{z}_{t+1}^{(1)}$ and the second vector $\mathbf{z}_{t+1}^{(2)}$ is orthogonal to $\mathbf{z}_{t+1}^{(1)}$. Through this GSR procedure, we numerically calculate the first and second Lyapunov exponents σ_1 and σ_2 of a trajectory segment with length L,

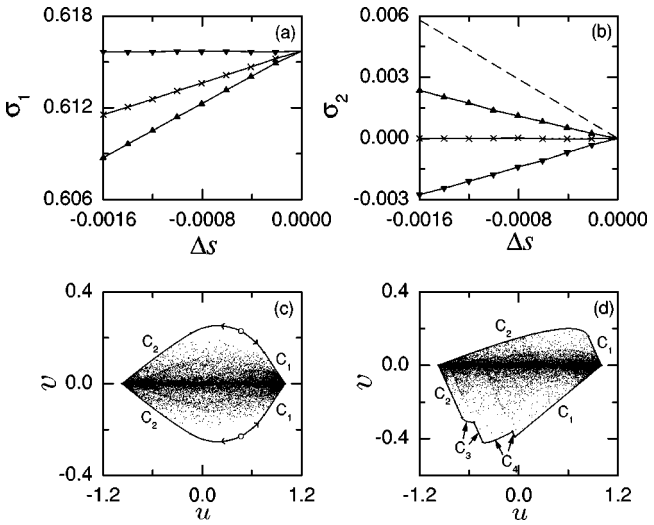

FIG. 2. Plots of the (a) first (σ_1) and (b) second (σ_2) Lyapunov exponents of the newly born asynchronous attractors born through supercritical blowout bifurcations vs the deviation Δs ($=s-s^*$) from the blowout bifurcation point s^* ($\simeq 0.2299$) for $a=1.97$ with $\alpha=0$ (up triangles), 0.852 (crosses), and 1 (down triangles). The length of a trajectory segment for the calculation of σ_1 and σ_2 is $L=10^8$, and straight line segments between neighboring data symbols are plotted only to guide the eye. For reference, the transverse Lyapunov exponent of the SCA, $\sigma_\perp$, is represented by a dashed line in (b). For $\Delta s=-0.0016$, examples of (c) hyperchaotic ($\sigma_1=0.6087$ and $\sigma_2=0.0024$) and (d) chaotic ($\sigma_1=0.6157$ and $\sigma_2=-0.0028$) attractors are given when $\alpha=0$ and 1, respectively. In both (c) and (d), the initial orbit point is $(u_0,v_0)=(0.5,0.01)$, 5×10^3 points are computed before plotting, and the next 4×10^4 points are plotted. In (c) segments of unstable manifolds (whose direction is denoted by arrows) of an asynchronous period-2 saddle (denoted by open circles) connect to segments of the critical curves C_k ($k=1,2$) (dots denote where these segments connect), and hence define a mixed absorbing area which a hyperchaotic attractor fills. In (d), a chaotic attractor fills an absorbing area bounded by segments of the critical curves C_k ($k=1,2,3,4$).

$$\sigma_1=\frac{1}{L}\sum_{t=0}^{L-1} r_t^{(1)}, \quad r_t^{(1)}=\ln d_{t+1}^{(1)}, \tag{12a}$$

$$\sigma_2=\frac{1}{L}\sum_{t=0}^{L-1} r_t^{(2)}, \quad r_t^{(2)}=\ln d_{t+1}^{(2)}, \tag{12b}$$

where $r_t^{(1)}$ ($r_t^{(2)}$) denotes the rate of exponential growth of the length of the first vector (the component of the evolved second vector orthogonal to the evolved first vector) at the time t. In this way, we obtain an approximation for the first and second Lyapunov exponents of the asynchronous attractor born through the blowout bifurcation.

Figures 2(a) and 2(b) show σ_1 and σ_2 of the asynchronous attractors born through blowout bifurcations for $\alpha=0$ (up triangles), 0.852 (crosses), and 1 (down triangles). For the case of unidirectional coupling ($\alpha=1$), σ_1 is just the longitudinal Lyapunov exponent $\sigma_{||}$ of the SCA. On the other hand, as α is decreased toward zero, the value of σ_1 becomes smaller [see Fig. 2(a)]. However, σ_1 is always positive for all α. For this case, the type of the asynchronous attractor with $\sigma_1>0$ is determined through the sign of σ_2. For the symmetric coupling case ($\alpha=0$), the asynchronous attractor is hyperchaotic with $\sigma_2>0$. On the other hand, as α is increased from zero, the value of σ_2 decreases, eventually it becomes zero for a threshold value α^* ($\simeq 0.852$), and then it becomes negative [see Fig. 2(b)]. Hence, an asynchronous chaotic attractor with $\sigma_2<0$ appears for $\alpha>\alpha^*$. As examples for $\Delta s(=s-s^*)=-0.0016$, see Figs. 2(c) and 2(d) that show the asynchronous hyperchaotic ($\sigma_1=0.6087$ and $\sigma_2=0.0024$) and chaotic ($\sigma_1=0.6157$ and $\sigma_2=-0.0028$) attractors when $\alpha=0$ and 1, respectively.

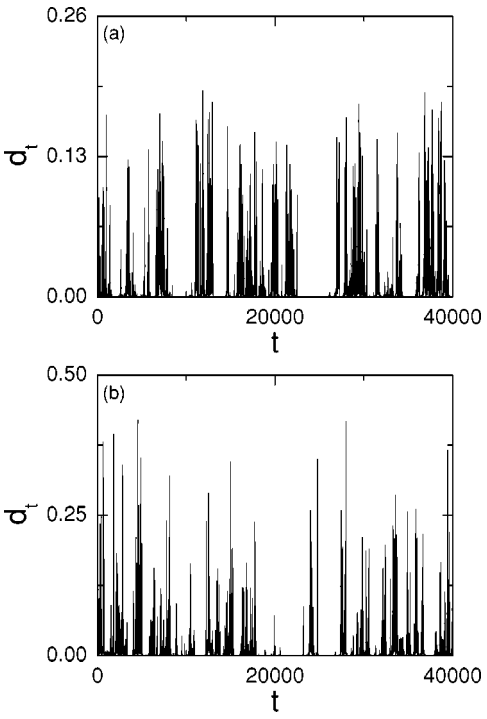

FIG. 3. Time series of the variable $d(=|v|)$, representing the deviation from the invariant $v=0$ line, for $a=1.97$ and $\Delta s=-0.0016$ with (a) $\alpha=0$ and (b) $\alpha=1$. In both cases, the initial orbit point is $(u_0,v_0)=(0.5,0.01)$.

As shown in Fig. 3, the time series of the variable d ($=|v|$) of typical trajectories on the newly born asynchronous attractors exhibits on-off intermittency, in which long episodes of nearly synchronous evolution are occasionally interrupted by short-term bursts. To characterize the on-off intermittent time series, we use a small quantity d^* for the threshold value of d such that for $d<d^*$ the signal is considered to be in the laminar (off) state and for $d\geqslant d^*$ it is considered to be in the bursting (on) state. So far, statistical properties of such on-off intermittent attractors have been well characterized through investigation of the distribution of the laminar lengths and the scaling of the average laminar length and the average bursting amplitude [14–20].

However, although examples were given in previous works (e.g., see Refs. [9,21–23]), the dynamical origin for the appearance of asynchronous hyperchaotic and chaotic intermittent attractors through blowout bifurcations remains unclear. Hence, we investigate the type of asynchronous in-

termittent attractors by varying the asymmetry parameter α. As explained above, a typical trajectory, exhibiting on-off intermittency, may be decomposed into its laminar and bursting components. Then the second Lyapunov exponent σ_2 of an asynchronous attractor [see Eq. (12b) for the second Lyapunov exponent of a trajectory segment] can be given by the sum of the two weighted second Lyapunov exponents of the laminar and bursting components, Λ_2^l and Λ_2^b:

$$\sigma_2 = \Lambda_2^l + \Lambda_2^b \tag{13a}$$

$$= \Lambda_2^b - |\Lambda_2^l|, \tag{13b}$$

where the laminar component always has a negative weighted second Lyapunov exponent ($\Lambda_2^l < 0$). Here, the weighted second Lyapunov exponent Λ_2^i for each component ($i = l,b$) is given by the product of the fraction μ_i of time spent in the i state and its second Lyapunov exponent σ_2^i, i.e.,

$$\Lambda_2^i = \mu_i \sigma_2^i; \quad \mu_i = \frac{L^i}{L}, \quad \sigma_2^i = \frac{1}{L^i} \sum_{t \in i\text{state}}{}' \; r_t^{(2)} \quad (i = l,b), \tag{14}$$

where L^i is the time spent in the i state for a trajectory segment of length L and the primed summation is performed in each i state. As can be seen in Eq. (13b), the sign of σ_2 is determined through competition of the laminar and bursting components. Hence, when the strength (i.e., the weighted second Lyapunov exponent Λ_2^b) of the bursting component is larger (smaller) than that (i.e., $|\Lambda_2^l|$) of the laminar component, an asynchronous hyperchaotic (chaotic) attractor appears. We also note that the weighted Lyapunov exponents Λ_2^l and Λ_2^b depend on the threshold value d^*, although σ_2 is independent of d^*. With decreasing d^*, Λ_2^l decreases to zero because the time μ_l spent in the laminar state goes to zero; thus Λ_2^b ($= |\Lambda_2^l| + \sigma_2$) converges to σ_2. Here, we again emphasize that σ_2, determining the type of asynchronous attractors, depends only on the difference between Λ_2^b and $|\Lambda_2^l|$, which is independent of d^* [see Eq. (13b)]. Hence, although $\Lambda_2^{l(b)}$ depends on d^*, the conclusion as to the type of asynchronous attractors is independent of d^*. Hereafter, we fix the value of the threshold value of d at $d^* = 10^{-5}$.

Figures 4(a) and 4(b) show the strength of the bursting and laminar components, Λ_2^b and $|\Lambda_2^l|$, respectively. As mentioned above, the type of newly born asynchronous attractor is determined through competition between the laminar and the bursting components as follows. We first note that for $\alpha = 0$ (up triangles), the bursting component is dominant, because $\Lambda_2^b > |\Lambda_2^l|$. However, as α is increased from zero, Λ_2^b decreases, while $|\Lambda_2^l|$ is nearly independent of α. Eventually, for a threshold value α^* [$\simeq 0.852$ (crosses)], the strength of the bursting and laminar components becomes balanced (i.e., $\Lambda_2^b = |\Lambda_2^l|$), and then the laminar component becomes dominant for $\alpha > \alpha^*$ [e.g., $\alpha = 1$ (down triangles)],

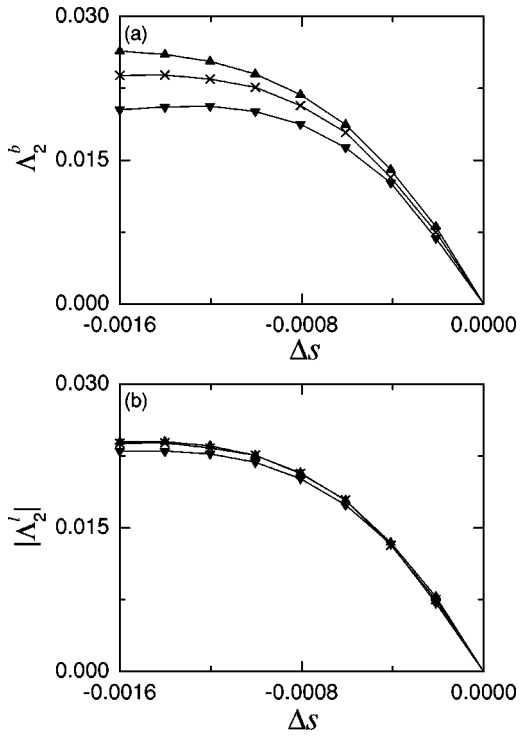

FIG. 4. Plots of strength of the (a) bursting and (b) laminar components [i.e., (a) Λ_2^b and (b) $|\Lambda_2^l|$] vs Δs ($= s - s^*$) for $a = 1.97$ with $\alpha = 0$ (up triangles), 0.852 (crosses), and 1 (down triangles). The threshold value of the variable $d(=|v|)$ is $d^* = 10^{-5}$, and straight line segments between neighboring data symbols are plotted just to guide the eye. Note that as α is increased from zero, Λ_2^b decreases, while $|\Lambda_2^l|$ is nearly independent of α.

because $\Lambda_2^b < |\Lambda_2^l|$. Consequently, for $\alpha < \alpha^*$, there is a hyperchaotic attractor with $\sigma_2 > 0$, while for $\alpha > \alpha^*$, there is a chaotic attractor with $\sigma_2 < 0$.

The fraction $\mu_{l(b)}$ of the laminar (bursting) time [i.e., the time spent in the laminar (bursting) state] and the second Lyapunov exponent $\sigma_2^{l(b)}$ of the laminar (bursting) component are also given in Fig. 5. For the case of the laminar component, both μ_l and σ_2^l are nearly independent of α, and hence its weighted second Lyapunov exponent Λ_2^l ($= \mu_l \sigma_2^l$) becomes nearly the same, independently of α. On the other hand, the second Lyapunov exponent σ_2^b of the bursting component decreases with increasing α from zero [$\alpha = 0$ (up triangles), 0.852 (crosses), and 1 (down triangles)], while its fraction μ_b ($= 1 - \mu_l$) of the bursting time is nearly independent of α. Consequently, the strength of the bursting component [i.e., $\Lambda_2^b (= \mu_b \sigma_2^b)$] becomes smaller as α is increased from zero. Thus, for a threshold value α^* ($\simeq 0.852$), the strength of the laminar and bursting components becomes balanced (i.e., $\Lambda_2^b = |\Lambda_2^l|$), and then a transition from asynchronous hyperchaos to chaos occurs.

We believe that the transition we have found from a hyperchaotic to a chaotic asynchronous attractor can be understood as follows. After the blowout bifurcation, the asynchronous attractor includes an infinite number of asynchronous unstable periodic orbits that are off the invariant line $v = 0$. Some of these unstable periodic orbits have

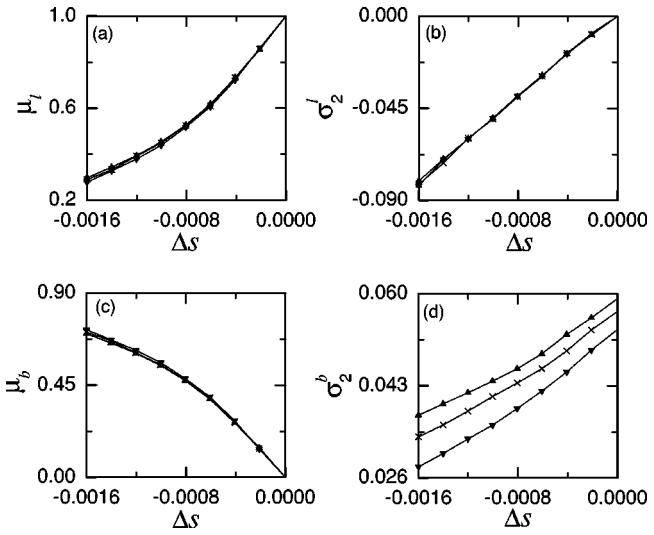

FIG. 5. Plots of (a) [(c)] the fraction $\mu_{l(b)}$ of the laminar (bursting) time and (b) [(d)] the second Lyapunov exponent $\sigma_2^{l(b)}$ of the laminar (bursting) component vs Δs $(=s-s^*)$ for $a=1.97$ with $\alpha=0$ (up triangles), 0.852 (crosses), and 1 (down triangles). The threshold value of the variable $d(=|v|)$ is $d^*=10^{-5}$, and straight line segments between neighboring data symbols are plotted only to guide the eye. Note that as α is increased from zero, σ_2^b decreases, while $\mu_{l(b)}$ and σ_2^l are nearly independent of α.

two positive Lyapunov exponents and some others have only one positive Lyapunov exponent. It is conjectured that as α increases from zero, the strength of the group of asynchronous unstable periodic orbits with negative second Lyapunov exponents might increase, which may result in the observed decrease in σ_2^b.

Finally, we discuss implication of the above results for the case of global coupling. The transition from synchronous chaos to asynchronous hyperchaos or chaos via a blowout bifurcation corresponds to a transition from a fully synchronized state to a two-cluster state in globally coupled 1D maps. Depending on the value of the parameter p (describing the distribution of elements between the two clusters), the intermittent two-cluster state is hyperchaotic or chaotic. The type of this intermittent two-cluster state may be determined through a competition between its laminar and bursting components. If the bursting (laminar) component becomes dominant, then a hyperchaotic (chaotic) two-cluster state appears.

B. Consequence of blowout bifurcations in high-dimensional invertible systems

Since the (noninvertible) 1D map is a paradigm model for period-doubling dynamics in a large class of systems, the results obtained in the preceding section are of wider significance. As examples, we consider coupled Hénon maps [17] and coupled parametrically forced pendula [28] which are high-dimensional invertible systems exhibiting period doublings and find similar results.

First, we consider two coupled Hénon maps, often used as a representative model for the Poincaré map of coupled oscillators:

$$x_{t+1}^{(1)}=f(x_t^{(1)})-y_t^{(1)}+(1-\alpha)c[f(x_t^{(2)})-f(x_t^{(1)})], \tag{15a}$$

$$y_{t+1}^{(1)}=bx_t^{(1)}, \tag{15b}$$

$$x_{t+1}^{(2)}=f(x_t^{(2)})-y_t^{(2)}+c[f(x_t^{(1)})-f(x_t^{(2)})], \tag{15c}$$

$$y_{t+1}^{(2)}=bx_t^{(2)}, \tag{15d}$$

where $(x_t^{(i)},y_t^{(i)})$ $(i=1,2)$ is a state vector of the ith subsystem at a discrete time t, $f(x)=1-ax^2$, c is a coupling parameter, α $(0\leqslant\alpha\leqslant1)$ is a parameter tuning the degree of asymmetry of coupling, and the Jacobian determinant of this system is b^2 $(|b|<1)$. As in the case of two coupled 1D maps, the two coupled Hénon maps may also be used as a model system for studying the two-cluster dynamics in many globally coupled Hénon maps.

As in the coupled 1D maps, we introduce new coordinates for the accuracy of numerical calculations,

$$u^{(1)}=\frac{x^{(1)}+x^{(2)}}{2},\quad u^{(2)}=\frac{y^{(1)}+y^{(2)}}{2},$$

$$v^{(1)}=\frac{x^{(1)}-x^{(2)}}{2},\quad v^{(2)}=\frac{y^{(1)}-y^{(2)}}{2}. \tag{16}$$

Then, the coupled Hénon maps of Eq. (15) become

$$u_{t+1}^{(1)}=1-a(u_t^{(1)2}+v_t^{(1)2})-2a\alpha cu_t^{(1)}v_t^{(1)}-u_t^{(2)}, \tag{17a}$$

$$u_{t+1}^{(2)}=bu_t^{(1)}, \tag{17b}$$

$$v_{t+1}^{(1)}=-2a[1-(2-\alpha)c]u_t^{(1)}v_t^{(1)}-v_t^{(2)}, \tag{17c}$$

$$v_{t+1}^{(2)}=bv_t^{(1)}. \tag{17d}$$

In this new map, we investigate the type of asynchronous intermittent attractors born via blowout bifurcations by varying the asymmetry parameter α when $b=0.1$ and $a=1.83$. Synchronous orbits lie on an invariant plane where $v^{(1)}=v^{(2)}=0$. When the scaled coupling parameter s $[=(1-\alpha/2)c]$ passes a threshold value s^* $(\simeq0.1787)$, the SCA on the invariant plane becomes transversely unstable, because its largest transverse Lyapunov exponent becomes positive. Then, a new asynchronous attractor appears through a supercritical blowout bifurcation. To calculate the Lyapunov exponents of the newly born asynchronous attractor, we choose a random value for $u_0^{(1)}$ with uniform probability in the range of $u_0^{(1)}\in(-0.5,0.5)$ and follow a trajectory starting from an initial orbit point $(u_0^{(1)},bu_0^{(1)},\varepsilon,b\varepsilon)$ $(\varepsilon=10^{-5})$ until its length L becomes 10^8. As shown in Fig. 6(a), the second Lyapunov exponent σ_2 of the asynchronous attractor depends on the asymmetry parameter α [$\alpha=0$ (up triangles), 0.905 (crosses), and 1 (down triangles)]. There exists a threshold value α^* $(\simeq0.905)$ such that for $\alpha<\alpha^*$ the asynchronous attractor is hyperchaotic with $\sigma_2>0$, while for $\alpha>\alpha^*$ it is chaotic with $\sigma_2<0$. Figures 6(b) and 6(c) show examples of the asynchronous hyperchaotic and cha-

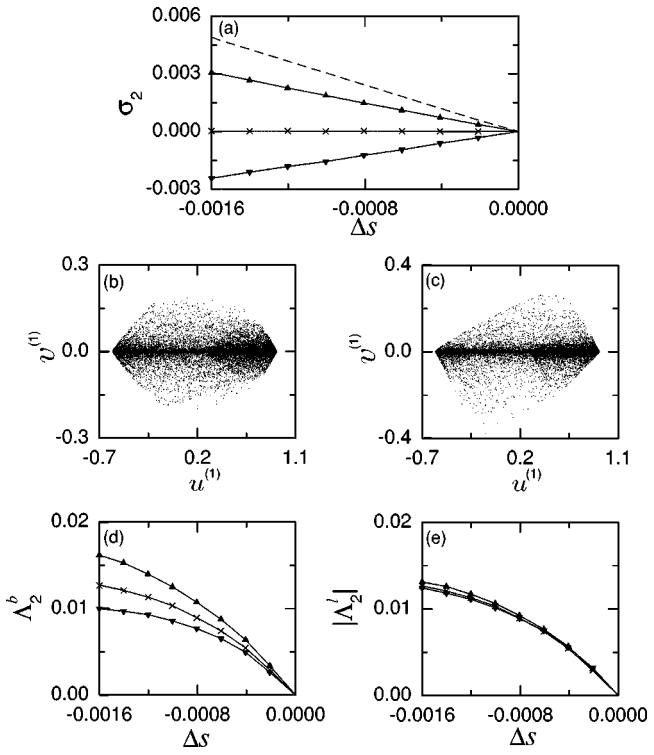

FIG. 6. Consequence of blowout bifurcations in two coupled Hénon maps for $b=0.1$ and $a=1.83$. When the scaled coupling parameter s passes a threshold value s^* $(=0.1787)$, an intermittent asynchronous attractor is born via a blowout bifurcation. The length of a trajectory segment for the calculation of the Lyapunov exponents of the asynchronous attractor is $L=10^8$ and the threshold value of the variable d $[=\frac{1}{2}(|v_1|+|v_2|)]$, representing the deviation from the invariant plane, is $d^*=10^{-4}$. (a) Plot of σ_2 vs Δs $(=s-s^*)$ for $\alpha=0$ (up triangles), 0.905 (crosses), and 1 (down triangles). The dashed line represents the largest transverse Lyapunov exponent of the SCA. Note that σ_2 depends on α. Projections of (b) hyperchaotic ($\sigma_1=0.4340$ and $\sigma_2=0.0031$) and (c) chaotic ($\sigma_1=0.4406$ and $\sigma_2=-0.0024$) attractors onto the $u^{(1)}$-$v^{(1)}$ plane are given for $\Delta s=-0.0016$ with $\alpha=0$ and 1, respectively. In both (b) and (c) the initial orbit point is $(u_0^{(1)},u_0^{(2)},v_0^{(1)},v_0^{(2)})=(0.5,0.05,0.01,0.001)$, the 5×10^3 points are computed before plotting, and the next 5×10^4 points are plotted. Plots of Λ_2^b and $|\Lambda_2^l|$ vs Δs are also given in (d) and (e), respectively. The symbols are the same as those in (a). For $\alpha<\alpha^*$ $(\simeq0.905)$, $\Lambda_2^b>|\Lambda_2^l|$, while for $\alpha>\alpha^*$, $\Lambda_2^b<|\Lambda_2^l|$. In (a), (d), and (e), straight line segments between neighboring data symbols are plotted only to guide the eye.

otic attractors for $\Delta s(=s-s^*)=-0.0016$ with $\alpha=0$ and 1, respectively. As in the coupled 1D maps, we use a threshold value d^* $(=10^{-4})$ for the variable d $[\equiv\frac{1}{2}(|v^{(1)}|+|v^{(2)}|)]$, representing the deviation from the invariant plane. When $d<d^*$, the system is said to be in the laminar (off) state, while for $d\geqslant d^*$ it is said to be in the bursting (on) state. As in Sec. II A we find that the type of an asynchronous intermittent attractor is determined through the competition between its laminar and bursting components [see Eq. (13b)]. Figures 6(d) and 6(e) show the strength of the bursting and laminar components (i.e., Λ_2^b and $|\Lambda_2^l|$), respectively. Note that as α increases from zero [$\alpha=0$ (up triangles), 0.905 (crosses), and 1 (down triangles)], Λ_2^b decreases, while $|\Lambda_2^l|$ is nearly independent of α. For $\alpha<\alpha^*$ $(\simeq0.905)$, the bursting component is dominant because $\Lambda_2^b>|\Lambda_2^l|$, and hence a hyperchaotic attractor with $\sigma_2>0$ appears. On the other hand, for $\alpha>\alpha^*$, a chaotic attractor with $\sigma_2<0$ appears because the laminar component becomes dominant (i.e., $\Lambda_2^b<|\Lambda_2^l|$).

As a second example, we consider a system of two coupled parametrically forced pendula:

$$\dot{x}_1=y_1+(1-\alpha)c(x_2-x_1), \tag{18a}$$

$$\dot{y}_1=f(x_1,y_1,t)+(1-\alpha)c(y_2-y_1), \tag{18b}$$

$$\dot{x}_2=y_2+c(x_1-x_2), \tag{18c}$$

$$\dot{y}_2=f(x_2,y_2,t)+c(y_1-y_2), \tag{18d}$$

where (x_i,y_i) $(i=1,2)$ is a state vector of the ith subsystem, $f(x,y,t)=-2\pi\beta\Omega y-2\pi(\Omega^2-A\cos2\pi t)\sin2\pi x$, x is a normalized angle with range $x\in[0,1)$, y is a normalized angular velocity, the overdot denotes a derivative with respect to time t, β is a normalized damping parameter, Ω is a normalized natural frequency of the unforced pendulum, A is a normalized driving amplitude of the vertical oscillation of the suspension point, c is a coupling parameter, and α is a parameter tuning the degree of the asymmetry of coupling. As in two coupled 1D maps, these two coupled parametrically forced pendula may also be used as a model for investigating the two-cluster dynamics in many globally coupled pendula.

As in the coupled Hénon maps, we introduce new coordinates,

$$u_1=\frac{x_1+x_2}{2},\quad u_2=\frac{y_1+y_2}{2},\quad v_1=\frac{x_1-x_2}{2},\quad v_2=\frac{y_1-y_2}{2}. \tag{19}$$

Then, the equations of motion of Eq. (18) become

$$\dot{u}_1=u_2+\alpha c v_1, \tag{20a}$$

$$\dot{u}_2=-2\pi\beta\Omega u_2-2\pi(\Omega^2-A\cos2\pi t)\times\sin2\pi u_1\cos2\pi v_1+\alpha c v_2, \tag{20b}$$

$$\dot{v}_1=v_2-(2-\alpha)c v_1, \tag{20c}$$

$$\dot{v}_2=-2\pi\beta\Omega v_2-2\pi(\Omega^2-A\cos2\pi t)\times\cos2\pi u_1\sin2\pi v_1-(2-\alpha)c v_2. \tag{20d}$$

The phase space of the coupled parametrically forced pendula is five dimensional with coordinates u_1, u_2, v_1, v_2,

and t. Since the system is periodic in t, it is convenient to regard time as a circular coordinate in the phase space. We also consider the surface of section, the u_1-u_2-v_1-v_2 hypersurface at integer times (i.e., $t=m$, m: integer). Then, using the fourth-order Runge-Kutta method with a time step $h=0.02$, we integrate Eq. (20) and follow a trajectory. This phase-space trajectory intersects the surface of section in a sequence of points. This sequence of points corresponds to a mapping on the 4D hypersurface. The map can be computed by stroboscopically sampling the orbit points $\mathbf{w}_m$ $[\equiv(u_1(m),u_2(m),v_1(m),v_2(m))]$ at the discrete time m. We call the transformation $\mathbf{w}_m \to \mathbf{w}_{m+1}$ the Poincaré map, and write $\mathbf{w}_{m+1}=P(\mathbf{w}_m)$. This 4D Poincaré map P has a constant Jacobian determinant of $e^{-4\pi\beta\Omega-4s}$, where s $[=(1-\alpha/2)c]$ is the scaled coupling parameter, and synchronous orbits lie on the invariant plane where $v_1=v_2=0$.

As an example, we consider the 4D Poincaré map P for the case of $\beta=1.0$, $\Omega=0.5$, and $A=0.85$. When the scaled coupling parameter s passes a threshold value s^* $(\simeq 0.324)$, a new asynchronous attractor appears through a supercritical blowout bifurcation, as the SCA on the invariant plane becomes transversely unstable (i.e., its largest transverse Lyapunov exponent becomes positive). To calculate the Lyapunov exponents of the newly born asynchronous attractor, we choose a random value for $u_1(0)$ $[u_2(0)]$ with uniform probability in the range of $u_1(0)\in(-0.15,0.15)$ $[u_2(0)\in(-0.5,0.5)]$ and follow a trajectory starting from an initial orbit point $(u_1(0),u_2(0),\varepsilon,\varepsilon)$ $(\varepsilon=10^{-5})$ until its length L becomes 10^7. As shown in Fig. 7(a), the second Lyapunov exponent σ_2 of the asynchronous attractor depends on the asymmetry parameter α [$\alpha=0$ (up triangles), 0.84 (crosses), and 1 (down triangles)]. For $\alpha<\alpha^*$ $(\simeq 0.84)$, the asynchronous attractor is hyperchaotic with $\sigma_2>0$, while for $\alpha>\alpha^*$, it is chaotic with $\sigma_2<0$. Examples of asynchronous hyperchaotic and chaotic attractors for $\Delta s=-0.006$ with $\alpha=0$ and 1 are given in Figs. 7(b) and 7(c), respectively. As in the coupled Hénon maps, the asynchronous attractor exhibits on-off intermittency, and hence its type may be determined through the competition between its laminar and bursting components [see Eq. (13b)]. Figures 7(d) and 7(e) show the strength of the bursting and laminar components, Λ_2^b and $|\Lambda_2^l|$, respectively. We note that as α is increased from zero [$\alpha=0$ (up triangles), 0.84 (crosses), and 1 (down triangles)], the strength of the bursting component (i.e., Λ_2^b) decreases, while the strength of the laminar component (i.e., $|\Lambda_2^l|$) is nearly independent of α. For $\alpha<\alpha^*$ $(\simeq 0.84)$, $\Lambda_2^b>|\Lambda_2^l|$, and hence a hyperchaotic attractor with $\sigma_2>0$ appears. On the other hand, for $\alpha>\alpha^*$, a chaotic attractor with $\sigma_2<0$ appears because $\Lambda_2^b<|\Lambda_2^l|$.

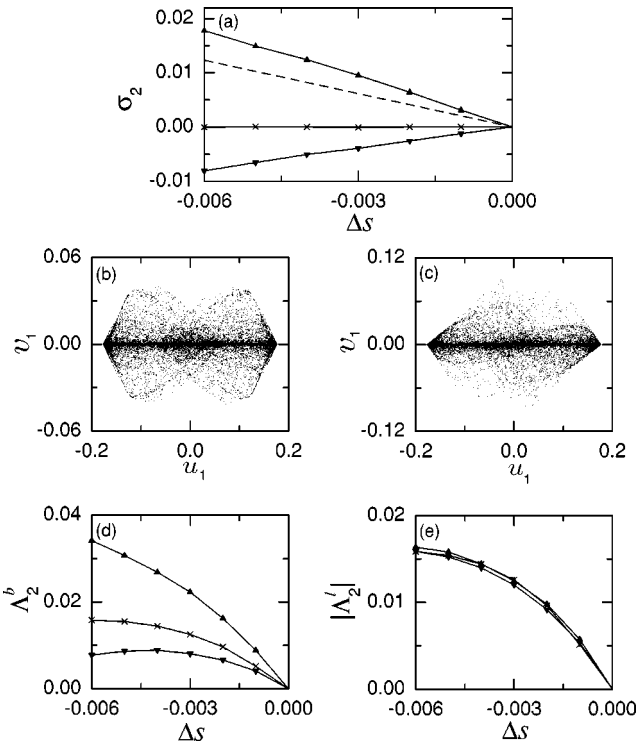

FIG. 7. Consequence of blowout bifurcations in two coupled parametrically forced pendula for $\beta=1.0$, $\Omega=0.5$, and $A=0.85$. When the scaled coupling parameter s passes a threshold value s^* $(\simeq 0.324)$, an intermittent asynchronous attractor is born via a blowout bifurcation. The length of a trajectory segment for the calculation of the Lyapunov exponents of an asynchronous attractor in the 4D Poincaré map P is $L=10^7$ and the threshold value of the variable d $[\equiv\frac{1}{2}(|v_1|+|v_2|)]$, representing the deviation from the invariant plane, is $d^*=10^{-4}$. (a) Plot of σ_2 vs Δs $(=s-s^*)$ for $\alpha=0$ (up triangles), 0.84 (crosses), and 1 (down triangles). The dashed line represents the largest transverse Lyapunov exponent of the SCA. Note that σ_2 depends on α. Projections of (b) hyperchaotic ($\sigma_1=0.628$ and $\sigma_2=0.017$) and (c) chaotic ($\sigma_1=0.648$ and $\sigma_2=-0.008$) attractors onto the u_1-v_1 plane are given for $\Delta s=-0.006$ with $\alpha=0$ and 1, respectively. In both (b) and (c), the initial orbit point is $(u_1,u_2,v_1,v_2)=(0.1,0.1,0.01,0.01)$, the 5×10^3 points are computed before plotting, and the next 3×10^4 points are plotted. Plots of Λ_2^b and $|\Lambda_2^l|$ vs Δs are also given in (d) and (e), respectively. The symbols are the same as those in (a). For $\alpha<\alpha^*(\simeq 0.84)$, $\Lambda_2^b>|\Lambda_2^l|$, while for $\alpha>\alpha^*$, $\Lambda_2^b<|\Lambda_2^l|$. In (a), (d), and (e), straight line segments between neighboring data symbols are plotted only to guide the eye.

III. SUMMARY

We have investigated the dynamical origin for the appearance of asynchronous hyperchaotic and chaotic attractors via blowout bifurcations in a representative model system of two coupled (noninvertible) 1D maps by varying the asymmetry parameter α. Note that the transition from synchronous chaos to asynchronous hyperchaos or chaos via a blowout bifurcation corresponds to a transition from a fully synchronized state to a hyperchaotic or chaotic two-cluster state in a system of globally coupled 1D maps. It has been found that the type of a newly born on-off intermittent asynchronous attractor (corresponding to an intermittent two-cluster state for the case of global coupling) is determined via competition between its laminar and bursting components. If the bursting (laminar) component becomes dominant, then an asynchronous hyperchaotic (chaotic) attractor [corresponding to a hyperchaotic (chaotic) two-cluster state for the globally coupled case] appears. Since the (uncoupled) 1D map represents a paradigm model for the period-doubling dynam-

ics in many systems such as forced oscillators, the above results are of wider significance. As examples, two coupled Hénon maps and two coupled parametrically forced pendula which are high-dimensional invertible period-doubling systems have been investigated and similar results have been found.

ACKNOWLEDGMENTS

This work was supported by the Korea Research Foundation (Grant No. KRF-2001-013-D00014), the U.S. Office of Naval Research (Physics), and the NSF (Grant No. PHYS-098632).

[1] K.M. Cuomo and A.V. Oppenheim, Phys. Rev. Lett. **71**, 65 (1993); L. Kocarev, K.S. Halle, K. Eckert, L.O. Chua, and U. Parlitz, Int. J. Bifurcation Chaos Appl. Sci. Eng. **2**, 973 (1992); L. Kocarev and U. Parlitz, Phys. Rev. Lett. **74**, 5028 (1995); N.F. Rulkov, Chaos **6**, 262 (1996).
[2] H. Fujisaka and T. Yamada, Prog. Theor. Phys. **69**, 32 (1983).
[3] A.S. Pikovsky, Z. Phys. B: Condens. Matter **50**, 149 (1984).
[4] V.S. Afraimovich, N.N. Verichev, and M.I. Rabinovich, Radiophys. Quantum Electron. **29**, 795 (1986).
[5] L.M. Pecora and T.L. Carroll, Phys. Rev. Lett. **64**, 821 (1990).
[6] P. Ashwin, J. Buescu, and I. Stewart, Nonlinearity **9**, 703 (1996).
[7] B.R. Hunt and E. Ott, Phys. Rev. Lett. **76**, 2254 (1996); Phys. Rev. E **54**, 328 (1996).
[8] E. Ott and J.C. Sommerer, Phys. Lett. A **188**, 39 (1994).
[9] P. Ashwin, P.J. Aston, and M. Nicol, Physica D **111**, 81 (1998).
[10] Y. Nagai and Y.-C. Lai, Phys. Rev. E **55**, R1251 (1997); **56**, 4031 (1997).
[11] P. Glendinning, Phys. Lett. A **264**, 303 (1999).
[12] A.S. Pikovsky and P. Grassberger, J. Phys. A **24**, 4587 (1991); A.S. Pikovsky, Phys. Lett. A **165**, 33 (1992).
[13] H. Fujisaka and T. Yamada, Prog. Theor. Phys. **74**, 918 (1985); **75**, 1087 (1986); H. Fujisaka, H. Ishii, M. Inoue, and T. Yamada, *ibid.* **76**, 1198 (1986).
[14] L. Yu, E. Ott, and Q. Chen, Phys. Rev. Lett. **65**, 2935 (1990); Physica D **53**, 102 (1992).
[15] N. Platt, E.A. Spiegel, and C. Tresser, Phys. Rev. Lett. **70**, 279 (1993); J.F. Heagy, N. Platt, and S.M. Hammel, Phys. Rev. E **49**, 1140 (1994); N. Platt, S.M. Hammel, and J.F. Heagy, Phys. Rev. Lett. **72**, 3498 (1994).
[16] S.C. Venkataramani, T.M. Antonsen, E. Ott, and J.C. Sommerer, Physica D **96**, 66 (1996).
[17] M. Ding and W. Yang, Phys. Rev. E **56**, 4009 (1997).
[18] H.L. Yang and E.J. Ding, Phys. Rev. E **50**, R3295 (1994).
[19] A. Čenys and H. Lustfeld, J. Phys. A **29**, 11 (1996).
[20] D. Marthaler, D. Armbruster, Y.-C. Lai, and E. Kostelich, Phys. Rev. E **64**, 016220 (2001).
[21] M. de Sousa Vieira, A.J. Lichtenberg, and M.A. Lieberman, Phys. Rev. A **46**, R7359 (1992).
[22] T. Kapitaniak, Phys. Rev. E **47**, R2975 (1993); T. Kapitaniak and L.O. Chua, Int. J. Bifurcation Chaos Appl. Sci. Eng. **4**, 477 (1994).
[23] S.-Y. Kim and W. Lim, Phys. Rev. E **64**, 016211 (2001); **63**, 026217 (2001).
[24] O. Popovych, Yu. Maistrenko, E. Mosekilde, A. Pikovsky, and J. Kurths, Phys. Lett. A **275**, 401 (2002); Phys. Rev. E **63**, 036201 (2001).
[25] I. Aranson, D. Golomb, and H. Sompolinsky, Phys. Rev. Lett. **68**, 3495 (1992); D. Auerbach, *ibid.* **72**, 1184 (1994); Y. Jiang and P. Parmananda, Phys. Rev. E **57**, 4135 (1998).
[26] D.J. Gauthier and J.C. Bienfang, Phys. Rev. Lett. **77**, 1751 (1996).
[27] P. Ashwin, J. Buescu, and I. Stewart, Phys. Lett. A **193**, 126 (1994).
[28] S.-Y. Kim and K. Lee, Phys. Rev. E **54**, 1237 (1996); S.-Y. Kim and W. Lim, *ibid.* **63**, 036223 (2001).
[29] D.V. Ramana Reddy, A. Sen, and G.L. Johnston, Phys. Rev. Lett. **80**, 5109 (1998).
[30] K. Wiesenfeld, P. Colet, and S.H. Strogatz, Phys. Rev. Lett. **76**, 404 (1996).
[31] C.S. Peskin, *Mathematical Aspects of Heart Physiology* (Courant Institute of Mathematical Sciences, New York, 1975).
[32] J. Buck, Q. Rev. Biol. **63**, 265 (1988).
[33] T.J. Walker, Science **166**, 891 (1969).
[34] K. Kaneko, Physica D **41**, 137 (1990); **75**, 55 (1994); **124**, 322 (1998).
[35] When the magnitude of a transverse variable d of an asynchronous trajectory, representing the deviation from the invariant synchronization line, is less than a threshold value $\tilde{d}$, the computed trajectory falls into an exactly synchronous state due to a finite precision [38]. In the system of coordinates x and y, the order of magnitude of the threshold value $\tilde{d}$ for $d\ (=|x-y|)$ is about 10^{-15} except the region near the origin, because the double-precision values of x and y have about 15 decimal places of precision. On the other hand, in the system of u and v, the order of magnitude of the threshold value $\tilde{d}$ for $d\ (=|v|)$ is about 2.2×10^{-308}, which is a threshold value for the numerical underflow in the double-precision calculation. Hence, in the system of u and v, we can follow a trajectory until its length becomes sufficiently long for the calculation of Lyapunov exponents of an asynchronous attractor.
[36] C. Mira, L. Gardini, A. Barugola, and J.-C. Cathala, *Chaotic Dynamics in Two-Dimensional Noninvertible Maps* (World Scientific, Singapore, 1996); R.H. Abraham, L. Gardini, and C. Mira, *Chaos in Discrete Dynamical Systems* (Springer, New York, 1997).
[37] Yu.L. Maistrenko, V.L. Maistrenko, A. Popovich, and E. Mosekilde, Phys. Rev. Lett. **80**, 1638 (1998); G.-I. Bischi and L. Gardini, Phys. Rev. E **58**, 5710 (1998).
[38] Due to the finite numerical precision, the computer compiler regards very small (nonzero) numbers as zeros when their magnitudes are less than a threshold value r^* for numerical underflow [$r^*\simeq2.2\times10^{-308}$ for IEEE (Institute of Electrical and Electronics Engineers) double precision]. Once the magnitude of the transverse variable v becomes less than r^*, the computed trajectory falls into an exactly synchronous state ($v=0$), and further bursting from the $v=0$ line cannot occur. As s approaches s^* from below, the probability of occurrence

of such a synchronous state increases. For this case, we choose another random initial orbit points and repeat the procedure for calcualting the Lyapunov exponents until a trajectory segment of length L $(=10^8)$ is obtained.

[39] A. Wolf, J.B. Swift, H.L. Swinney, and J.A. Vastano, Physica D **16**, 285 (1985); G. Benettin, L. Galgani, A. Giorgilli, and J.-M. Strelcyn, Meccanica **15**, 9 (1980); A.J. Lichtenberg and M.A. Lieberman, *Regular and Stochastic Motion* (Springer-Verlag, New York, 1983), p. 283.